Journal of Atmospheric and Solar–Terrestrial Physics 225 (2021) 105760

Contents lists available at ScienceDirect

Journal of Atmospheric and Solar-Terrestrial Physics

journal homepage: www.elsevier.com/locate/jastp

Estimating the electron energy and the strength of the electric field within sprites using ground-based optical data observed over South African storms

Stanislaus Nnadih [a,b,*], Michael Kosch [a,c,d,e], Janusz Mlynarczyk [f]

[a] South African National Space Agency, Hermanus, South Africa
[b] African Regional Centre for Space Science and Technology Education in English, Ife, Nigeria
[c] Department of Physics, Lancaster University, Lancaster, UK
[d] Physics and Astronomy, University of the Western Cape, Bellville, South Africa
[e] School of Chemistry and Physics, University of KwaZulu-Natal, Westville, South Africa
[f] AGH University of Science and Technology, Department of Electronics, Krakow, Poland

ARTICLE INFO

Keywords:
Lightning discharges
Sprites electron energy
Mesosphere
Thunderstorms

ABSTRACT

We present a new simplified method to estimate the characteristic electron energy and electric field within a mesospheric transient luminous event using ground-based calibrated and filtered optical data. We assume non-relativistic motion, a Maxwell-Boltzmann distribution, a model of the electron-neutral collision frequency, elastic electron collisions, that the collisional excitation cross-section can be assigned to a single value, and that each electron-neutral collision produces one photon on average. Example observations of carrot sprites over South Africa give estimated electron energy of 4.6–4.9 ± 0.03 eV, which compares favourably with previous similar results using more sophisticated methods. Ideally, two wavelengths should be observed simultaneously but we show a good estimate is possible with only the bright N2(1 PG) red emission.

1. Introduction

Sprites are transient luminous events, which occur in the stratosphere and mesosphere (Barrington-Leigh and Inan 1999; Sato et al., 2015) following strong positive (Sentman et al., 1995; Winckler et al., 1999; Liu et al., 2015), and in some cases negative (Barrington-Leigh 2001; Suzuki et al., 2006; Chen et al., 2019) Cloud-to-Ground lightning discharges in the troposphere. Since their discovery in the late 1980s (Franz et al., 1990), there have been several studies conducted from Space (Frey et al., 2016; Sato et al., 2015; Neubert et al., 2008) and Ground-based systems (Sentman et al., 1995; Neubert et al., 2001; Yair et al., 2004; Williams et al., 2010; Yaniv et al., 2013; Nnadih et al., 2018) that used various techniques to describe the fleeting nature of sprites.

When observed with a colour imager, sprites tend to have an upper red portion at an altitude ~70–85 km, and a downwards wispy faint blue tendril that extends towards the top of the cloud. Spectral measurement of sprites in the optical bandpass of 400–800 nm (Mende et al., 1995; Hampton et al., 1996), reveal that whilst the red appearance originates from electron impact excitations of the first positive nitrogen neutral transitions (N_2(1 PG)), the blueish tendrils results from a combination of the first negative emissions of nitrogen ions (N_2^+(1NG)), and the second positive emissions in neutral nitrogen (N_2(2 PG)) (Hampton et al., 1996; Armstrong et al., 1998; Suszcynsky et al., 1998). Ground-based photometric studies by Armstrong et al. (1998) and Suszcynsky et al. (1998) shows that the blue emission from sprites has shorter durations (~5 ms) when compared to the red emissions, which can last up to ~ 100 ms (Heavner et al., 2010), and that the shorter duration of the blue emission is a function of a shorter lifetime due to quenching, which in addition to the atmospheric extinction in the blue, due to Rayleigh scattering, makes it difficult to observe the blue emissions from sprites using ground-based systems.

Whilst the space-based spectral observations of the 2PG/1NG emissions of sprites (Kuo et al., 2005) reveal characteristic electron energy that range from 4.5 to 6.5 eV, the aircraft based measurement (Morrill et al., 2002), which used a model that solves the Boltzmann equations as a function of the electric field, suggested that sprites electron characteristic energy above and below 55 km altitude is around ~ 1.75 eV and ~2.2 eV, respectively. In both cases, the electron energy is relatively low and non-relativistic. Photometric observations of sprites also show that the electron energies at the lower part of sprite halo range between 6 – 23 eV, suggesting that during sprites evolution, energetic processes occur at the initiation phase of sprites halo (Miyasato et al., 2003), and

* Corresponding author. South African National Space Agency, Hermanus, South Africa.
E-mail address: snnadih@sansa.org.za (S. Nnadih).

https://doi.org/10.1016/j.jastp.2021.105760
Received 30 January 2021; Received in revised form 9 July 2021; Accepted 14 September 2021
Available online 20 September 2021

there are strong correlations between electron energies within sprites events and the Charge Moment of the initiating parent lighting (Takahashi et al., 2009)

In this paper, we used a simplified approach to estimate the strength of the electric field and the characteristic electron energy within sprites using ground-based optical data recorded in southern Africa. In particular for ground-based observations when only N_2(1PG) observations are available, we show that a result consistent with previous work is possible.

2. Observations

2.1. Instrument

Sprite observing optical instruments were set up at Klerefontein farm near Carnarvon, South Africa (21.9803 E, 30.9715 S) to observe sprites during the austral summer of 2017/2018. The instruments consist of two optical cameras; a WATEC 910Hx and an iXon Andor EMCCD camera. The WATEC 910Hx is a quasi-linear, low-light monochromatic Charge Coupled Device (CCD) that has a threshold illumination of $5.1X10^{-6}$ Lux and a 0.5-inch interline image sensor (Astroshop Eu, 2018), which is commonly used for sprites research around the world (Mashao et al., 2021; Nnadih et al., 2018; Soula et al., 2009; Yaniv et al., 2013). The camera was fitted with an 8.0 mm f/1.4 lens, which gave a field of view (FOV) of 43° X 33° and was operated at a frame rate of 25 Hz. The iXon Andor EMCCD is a single photon counting camera (Andor Technical manual 2018) that amplifies weak signals to a level that can be detected by the CCD. The camera has a 1-inch image sensor, fitted with a 50 mm/f0.85 lens, and was operated at 50 fps and 256 X 256-pixel mode, with a 2 X 2 internal binning that allowed an acceptable trade-off between temporal and spatial resolution.

In order to observe a specific wavelength range of emissions from the sprites events, the WATEC 910Hx and the iXon Andor EMCCD camera's lens were fitted with a filter that has a spectral bandpass of 635–675 nm (for red emission) and 426–440 nm (for blue emission), respectively. The filters are standard nitrogen emission filters that cover the first positive nitrogen neutral emission (N2(1 PG) and ionized (N2+(1NG) emission spectrum of sprites. These optical instruments were mounted on a tripod and connected to a computer that ran the sprites capture software.

2.2. Observations

The storm, which was approximately 12–14 km high inferred from radiosonde data (FABL, station 68442) that was less than 100 km away from the location of the storm, had a cloud-top temperature that ranged between −49 °C and −57 °C as shown in Fig. 1. The storm was approximately 500 km from the observing point and had an active area that was about 21,200 km^2.

Fig. 2 shows the sprite events, observed at 635–675 nm that were further analysed in this paper. The observed sprites appear at a lower elevation in the image frame because of their distance to the observer. These events were between 554 and 613 km from the observation point. As a result of which, the iXon EMCCD camera that had the blue filter was not able to record any of the events because of the poor atmospheric transmission of the blue wavelength due to Rayleigh scattering at the lower viewing elevation. Since these events were observed from a single site, its location information was based on the position of the corresponding lightning stroke as retrieved from the lightning stroke data of the South African Lightning Detection Network (SALDN), which is operated by the South African Weather Service.

3. Data analysis

The sprite image frames were geolocated using the Sprite Analyser software that was developed by Sonotaco Inc. The software has the star coordinates from the SKY2000 Master Catalogue version 4 (Doug Mink Yale bright Star Catalogue, 2010). To determine the approximate coordinate (Latitude, longitude) of the sprites events, we manually overlaid approximately 47 background stars on the sprites images, from the reference stars in the star catalogue of the Sprite Analyser software. This was done with the assumption that the sprites were above their respective causative lightning discharge. The sprites luminosities maximum vertical height was approximately 85 ± 5 km, calculated using the law of sines techniques described by Füllekrug et al. (2019), where the elevation of the camera above sea level at the observation site (Carnarvon, South Africa) was 1308 m. The uncertainty from the manual alignment of these stars results from the star image pixel jitter (1-pixel, which is equivalent to 0.09°) in the vertical and horizontal direction.

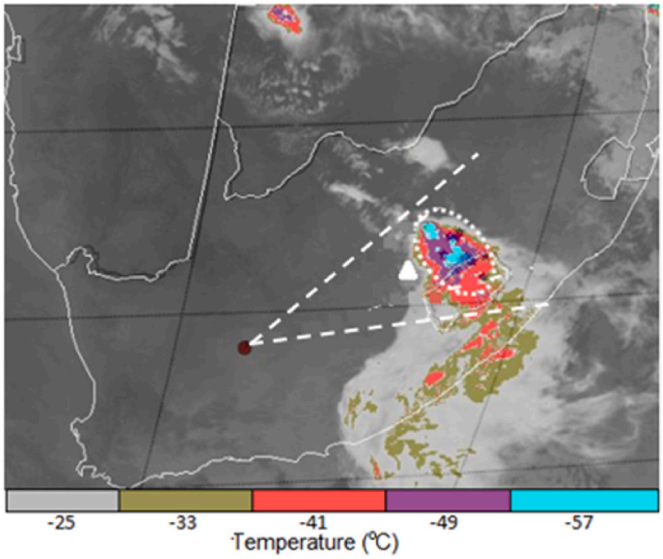

Fig. 1. The MeteoSat infrared imagery of the thunderstorm observed from Klerefontein farm on the 31st January 2018. The red dot shows the observation site; the dashed lines show the camera's field of view, while the dotted circle shows the sprites active section of the storm. The black asterisks within the dotted circle are the positions of the observed sprite events. The white triangle shows the location of the FABL sounding instrument (station 68442).

3.1. Estimation of the sprite's electron fluxes at various altitudes

In order to estimate the electron fluxes within sprites at various altitudes, we used the sprites images that contained at least one of the calibrated stars in the Yale Bright Star Catalog (Doug Mink Yale bright Star Catalogue, 2010). This enabled us to relate the flux of a known entity (the star) to the sprite's events, assuming quasi-linearity, since the background stars on the sprites images and the sprites events were recorded on the same night, using the same camera gain setting with the same atmospheric loss.

We then average the scintillation effect of the stars to determine an average intensity value ($Star_{avg}$) because stars have constant brightness. We later applied a 7 X 7 median filter on the sprites image frame to remove all the background stars. Since the maximum and minimum vertical heights of the sprite luminosities are around 85 ± 5 km and 40 ± 5 km respectively, which suggests that sprites vertical luminous emission profile height is approximately 40 km ± 5 km, we then divided this vertical luminous emission profile into equal sections with the assumption that each section spans approximately 10 km in the vertical. Thereafter, we measured the average pixel value of each of these sections that comprise of a superposition of sprites events and some background sky ($Sp + Sky_{bkg}$) and also the average Sky background pixel value ($SkyBk_{avg}$) of two adjacent areas of the sky without the sprite's

Fig. 2. Sprites events observed at a wavelength range of 635–675 nm. These events were recorded on the 31st January 2018 at (A) 23:11:30.8 UTC, (B) 23:51:11.6 UTC and (C) 22:53:17.3 UTC, respectively. The white dots around and above the sprites images are stars that were used to calibrate the images. The dark lower section shows the mountain (high plains) at the horizon. The sprite event on the right side in panel A was used for the analysis whilst in panel C, the sprites event on the left was used. The elevation to the brightest part of the sprites is approximately 4°, 3° and 5° for the event in panels A, B and C, respectively

events, but at the same altitude of each Sp + Sky_{bkg}. We later subtracted Sp + Sky_{bkg} from $SkyBk_{avg}$ to derive the emissions of sprites events at each altitude.

Finally, we used equation 1 to infer the flux of photons within sprites at various altitude shown in Table A1 (Appendix).

$$Sprites_{flux} = \frac{Star_{flux}\left(Sprites_{avg_{brightness}} - Sky_{bkg}\right)}{Star_{avg} - Sky_{bkg}}\left(ph\,/\,m^2\,/\,s\right) \qquad \text{Equation. 1}$$

Where this is integrated over the passband wavelength range of the filter,

$$Star_{flux} = \frac{Star_{power}}{Energy_{photon}}\left(\text{watt}/\text{m}^2\right)$$

and the $Star_{power}$ is obtained from the Yale Bright Star Catalogue (Doug 2010)

Fig. 3 shows the calibrated N2(1 PG) emission profile of sprites events as a function of altitude, for the three analysed events, where the image "2A", "2B" and "2C" of Fig. 2 relates to panels 3A, 3B and 3C, respectively.

These plots suggest that the N2 photon emission within sprites peak around 65–75 km, for which the fluxes of the electrons were estimated. The region (65–75 km) corresponds to sprites initiation altitudes before its downwards and then upwards development at speed of around 10^7 m/s (Lyons, 2015), and also agrees with airborne and other ground-based measurements (Sentman et al., 1995; Neubert et al., 2001; Füllekrug et al., 2019), which suggest that sprites obtain their maximum brightness around 68 km. The plots also show that a significant portion of the observed emission in sprites is produced in the body of sprites streamer.

The uncertainty associated with this estimate results from the image pixel jitter in the vertical direction, and the deviation between the maximum and minimum pixel values that were used whilst estimating the fluxes of the photons within sprites.

The ELF signal associated with the sprites was recorded at the Hylaty ELF station in Poland [Kulak et al., 2014]. The station records the magnetic field component of the EM field in the frequency range 0.03–300 Hz. The current moment waveform and charge moment change (CMC) were calculated using the method presented by Mlynarczyk et al. (2015) and the ELF propagation model described by Kulak and Mlynarczyk (2013), which suggests that the CMC associated with these events are 1057 C km, 2214 C km and 1930 C km for the events in panels 2A, 2B and 2C, respectively.

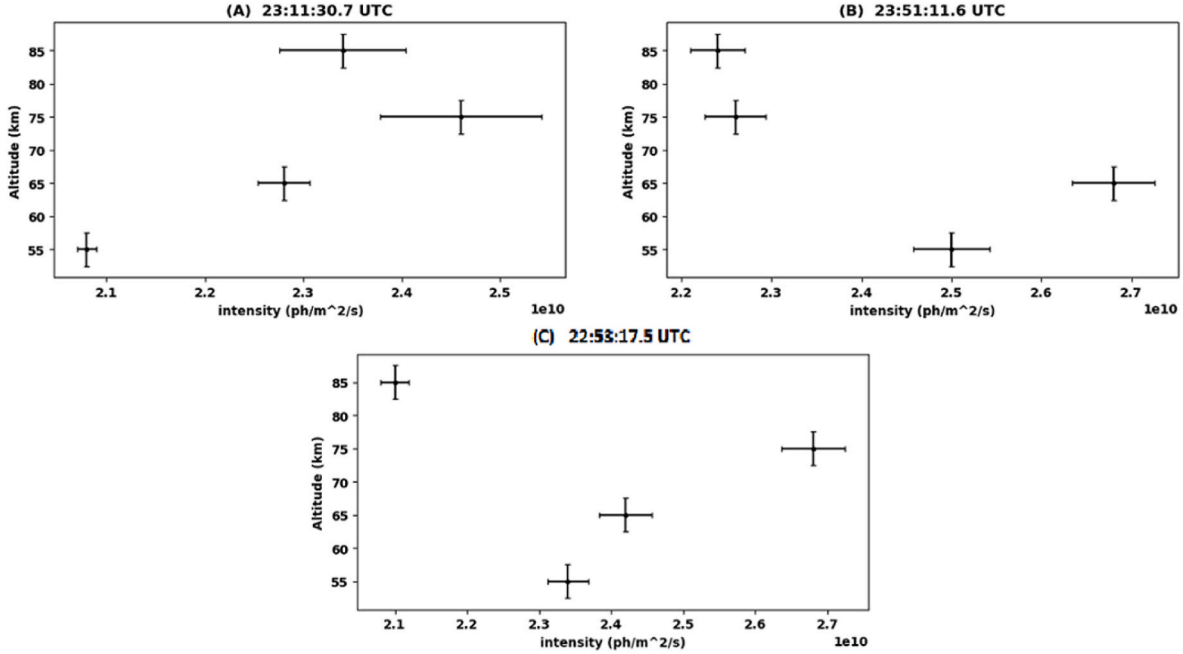

Fig. 3. The N2(1 PG) emission profile for sprites events observed at 635–675 nm.

3.2. Estimation of the characteristic electron energies within sprites at various altitudes

The characteristic electron energy is the average energy of the electrons in a weakly ionized gas, under an applied electric field (Heavner et al., 2010). In order to estimate this parameter, within sprites emission, we used the Maxwell-Boltzmann distribution function for collisional gases that describes particle speed in gas, where the particles do not constantly interact with each other but move freely between short collisions (Tec 2019). We equally made a few assumptions, which includes: (1) The electron(s) that were responsible to produce the red and blue photon(s) could be assigned to single energy in the collisional excitation cross-sections. (2) Every electron that collided with a neutral produces one photon per collision, and that the photon was above the detecting threshold of the camera. (3) Electron collisions are elastic. (4) Quenching effects are ignored. (5) The blue emissions from sprites events were not recorded because the emissions were below the sensitivity threshold of the camera. We show the characteristic energy estimate is not very sensitive to estimates of this emission intensity.

The Maxwell-Boltzmann distribution function of electron velocity in a collisional plasma, as in the case for the mesosphere, is given by:

$$f(v) = \sqrt{2} \Big/ \pi \left(\frac{m}{KT}\right)^{3} v^{2} exp\left(\frac{-mv^{2}}{2KT}\right) \quad \text{Equation 2}$$

where m is the mass of the electron, T is the temperature in Kelvin, K is Boltzmann constant and v is velocity.

Re-writing equation (2) to derive the energy term (Q),where energy $Q = \frac{3}{2}KT = \frac{1}{2}mv^{2}$

Equation (2) can be rearranged as:

$$f(v) = KQexp\left[\frac{-Q}{Q_o}\right] \quad \text{Equation 3}$$

where f(v) is the flux of electrons within sprites at various altitudes, K is the constant of proportionality, Q is the energy of the electrons and Q_o is the characteristic electron energy, which is the average energy of the electrons in a weakly ionized gas.

Assuming each electron-neutral collision produces one photon on average, the flux of the photons that produced the red emissions $(f(v)_r)$ in sprites is shown in Table A1(Appendix). Since we were not able to observe the blue emissions from sprites, we presume that the flux of the photons that would have produced observable blue photon emissions was just below the camera sensitivity threshold.

We then assigned all the electrons that produced the red(Q_r) and blue (Q_b) emissions to single energy, within the corresponding collisional excitation cross-section, i.e. Qr = 10 eV and Qb = 30 eV, respectively. Hence, equation (3) was modified to relate to the fluxes of the electrons that produced the photons that would be observed by the red and blue filtered cameras.

$$f(v)_r = KQ_r exp\left[\frac{-Q_r}{Q_o}\right] \quad \text{Equation 4}$$

$$f(v)_b = KQ_b exp\left[\frac{-Q_b}{Q_o}\right] \quad \text{Equation 5}$$

Assuming the EMCCD has a quasi-linear camera response, we used the calibrated stars to determine the camera's photon flux detection threshold as 1.2 X 10^8 ph/m^2/s, and assign this value to the blue photon flux in equation (5). Finally, we simultaneously solve equations (4) and (5) to determine the characteristic electron energies (Q_o) within sprites emissions, which range between 4.6 and 4.9 ± 0.03 eV (See Table A2 (Appendix).

In order to ascertain if the derived characteristic electron energy depends strongly on the blue emissions from sprites, we assigned half and a quarter of the value of the derived camera sensitivity threshold to blue emissions from sprites $(f(v)_b)$. The estimated values for the three analysed events range from 4.0 to 4.2 ± 0.03 eV and 3.5 to 3.7 ± 0.03 eV for the half and a quarter of the threshold valuerespectively, as shown in Table A3 (Appendix). This shows that the simplified technique used to determine Q_o does not depend strongly on the blue optical emissions from sprites that are attenuated to ground-based measurements. This is presumably due to the low flux of electrons above the energy threshold (18.6 eV) for the blue emission

3.3. Electric field estimation within sprites at various altitudes

Whilst neglecting ions, we assumed that the electric field is the only force that acted on the electrons.

$$F = ma = Eq, E = q/ma \quad \text{Equation 6}$$

Where F is the force, m is the mass of the electrons, a is acceleration, q is the charge of the electrons and E *is* the electric field.

We assume that the electron motion is non-relativistic (substantiated by low energy) and that the collision between the electron and neutrals is elastic. i.e.

$$Q_0 = \frac{1}{2}mv^{2} \Rightarrow v = \frac{\sqrt{2Qo}}{m} \quad \text{Equation 7}$$

and also that the electrons started from rest following each collision, i.e.

$$v = at \Rightarrow a = vV \quad \text{Equation 8}$$

Where v is the velocity of the electrons, Q_o is the characteristic energy of the electrons at various altitude, t is the collision time between the electrons, which is inversely proportional to the collision frequency (V) of the electrons at various altitudes. The collision frequency of the electrons at various altitudes shown in Table A4 (Appendix) was adapted from Kane (1959).

Substituting equation (7) into equation (8), we have

$$a = v\frac{\sqrt{2Q}}{m} \quad \text{Equation 9}$$

We derived equation (10) by substituting equation (9) into equation 6

$$E = \frac{q}{v\sqrt{2Qm}} \quad \text{Equation 10}$$

Which was finally used to determine the strength of the electric field within sprites at various altitudes of derived Q_o (Table A2), and estimated collision frequency of the electrons (Table A4). These values are shown in Table A5 (Appendix) Fig. 4 (A, B, C) shows a plot of the electric fields as a function of altitude, for the 3 analysed sprites events. Fig. 4D shows the average electric field from panels A–C, with the nominal conventional electric breakdown of pure dry air, derived from equation (11) (Surkov and Hayakawa 2012)

$$E_k = \frac{32N_m}{N_o}\ (kVcm-1) \quad \text{Equation 11}$$

Where N_m is the number of neutral gas particles at constant gas temperature (T) that was derived from the MSIS-E−90 Atmospheric Model (Hedin, 1991) for the day/time of the sprites campaign. N_o equals 2.7 x10^{25} m^{-3}, is the constant of the order of air number density at ground level (Surkov and Hayakawa 2012).

Fig. 4 A—C shows that the strength of the electric field within sprites increases with a decrease in altitude because the electron collision frequency increases as the neutral density increase at the lower altitudes. However, Fig. 4D suggests that our estimations may have some limitations at the lower altitudes when compared to the model. This discrepancy may have occurred as a result of the illumination from parent lightning flash from the top of the cloud as can be seen in Fig. 2, or because we neglected quenching effects which become more important

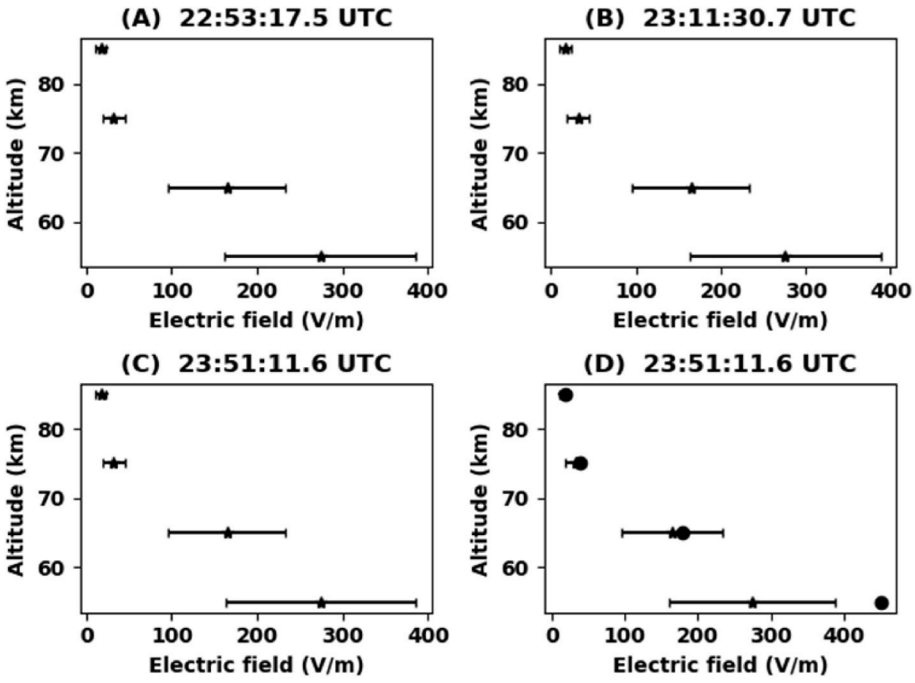

Fig. 4. Panels A, B, C show the derived electric field within sprites as a function of altitude, for the analysed events. Panel D shows the average sprites electric field in panels A–C, superimposed over the electric breakdown of pure dry air (black dots) derived from a model.

at lower altitudes.

4. Discussion and conclusion

The study used a simplified approach to estimate the characteristic electron energy and the strength of the electric field within sprites emissions. This was achieved by calibrating the emissions of sprites events as recorded by the camera to the flux of known stars in the star catalogue. For the three analysed events, the fluxes of the photons within sprites when observed in the wavelength range of 635–675 nm peaked around 70 km ± 5 km. This also supports earlier studies (Sentmann et al., 1999; Neubert et al., 2008; Bor, 2013; Füllekrug et al., 2019), which shows that sprites achieve their maximum brightness around 68 km.

The energy of the electrons within sprites emissions, for the three analysed events, was approximately 4.6–4.9 ± 0.03 eV. This value was estimated whilst presuming that electrons colliding with neutrals produces one photon per collision that was above the detection threshold of the camera. However, there are conditions where the excited neutral/ion may de-excite through collisions with other molecules whilst producing no photon. These situations, known as quenching, which occur as a result of the local atmospheric density (Ihaddadene and Celestin 2017), were not considered in this study. This may explain the difference in the electric field at the lower altitude compared to the model, and also shows that our simplified model maybe only valid above approximately 65 km altitude as quenching will increase at lower altitudes.

The estimated characteristic electron energy within sprites was comparable to space-based measurement (4.5–6.5 eV) inferred using a more complex approach that related a model result to observed data from space (Kuo et al., 2005). However, both the space-based measurement and our ground-based estimations were about twice the values (1.75–~2.2 eV) inferred from the airborne system (Morrill J., 2002). The aircraft-based measurement uses the blue (N2+(1NG)) emission data from sprites, which are absorbed less at aircraft altitude to estimate the sprite's characteristic electron energies at 55 km altitude and above. Our study shows that it is also possible to estimate the energy of the electron within sprites emission without the blue emissions data that are attenuated by Rayleigh scattering for ground-based optical systems.

The electric field within sprites was estimated by assuming that the motion of the electrons was non-relativistic and their collisions with neutrals species in the atmosphere were elastic. This suggests that for the analysed events, the strength of the electric field within sprites increases with a decrease in altitude, which also correlates with the expected dielectric breakdown of the atmosphere except at the lowest altitudes.

Declaration of competing interest

The authors declare that they have no known competing financial interests or personal relationships that could have appeared to influence the work reported in this paper.

Acknowledgement

The authors acknowledge the financial assistance of these funding organisations; the National Research Foundation (South Africa) through grant no. 12774, and the National Science Center (Poland), under grant no 2015/19/B/ST10/01055. The authors also wish to thank the South African Weather Service and the Climate System Analysis Group, Department of Environmental and Geographical Science, University of Cape Town, for their support during the study. The simulation results have been provided by the Community Coordinated Modeling Center at Goddard Space Flight Center through their public Runs on Request system (http://ccmc.gsfc.nasa.gov). The MSIS-E-90 Atmosphere Model was developed by A. E. Hedin at NASA, GSFC. The authors also thank the manuscript reviewers for their valuable contributions.

Appendix

Table A1
The flux of photons within sprites at various altitude observed at specific wavelength range (635–674 nm)

Altitude (km)	Fluxes of the photons (ph/m^2/s)		
	Event time: 23:11:30.7 UTC	Event time: 23:51:11.6 UTC	Event time: 22:53:17.5 UTC
85	2.34E+10	2.24E+10	2.10E+10
75	2.46E+10	2.26E+10	2.68E+10
65	2.20E+10	2.68E+10	2.42E+10
55	2.08E+10	2.50E+10	2.34E+10

Table A2
The estimated characteristic electron energies (Q_o) within sprites emissions at various altitudes for the three analysed events.

Altitude (km)	Characteristic electron energy(eV)		
	Event time: 23:11:30.7 UTC	Event time: 23:51:11.6 UTC	Event time: 22:53:17.5 UTC
85	4.79	4.84	4.92
75	4.73	4.83	4.64
65	4.86	4.64	4.75
55	4.93	4.72	4.79

Table A3
The characteristic electron energies within sprites events at various altitudes assuming a half, and a quarter of the camera's sensitivity threshold to blue emission from sprite events.

Altitude (km)	Event time: 23:11:30.7 UTC		Event time: 23:51:11.6 UTC		Event time: 22:53:17.5 UTC	
	Q_o		Q_o		Q_o	
	Half the camera's sensitivity threshold	Quarter the camera's sensitivity threshold	Half the camera's sensitivity threshold	Quarter the camera's sensitivity threshold	Half the camera's sensitivity threshold	Quarter the camera's sensitivity threshold
85	4.11	3.60	4.15	3.62	4.20	3.66
75	4.07	3.60	4.14	3.62	4.00	3.51
65	4.20	3.64	4.00	3.51	4.08	3.58
55	4.21	3.67	4.05	3.55	4.12	3.60

Table A4
The collision frequency of the electrons at various altitude (Adapted from Kane (1959)).

Altitude (km)	Collision frequency of electrons (V) Sec^{-1}	Collision time between electrons (t = 1/f) Sec
80	(2.3 ± 1.2) E+06	4.34 E−07
75	(4.3 ± 2.1) E+06	2.32E-07
65	(2.2 ± 0.5) E+07	4.50E-08
55	(3.6 ± 1.8) E+07	2.70E-08

Table A5
The estimated strength of the electric field within sprites at various altitudes.

Altitude(km)	Electric field strength within sprites (V/m)		
	Event time: 23:11:30.7 UTC	Event time: 23:51:11.6 UTC	Event time: 22:53:17.5 UTC
85	17.07	17.09	17.13
75	31.86	31.87	31.88
65	164.72	164.43	164.49
55	275.43	274.92	274.50

References

Andor Technology, 2018. Solis Software Packages. Technical report. Andor Technology.

Armstrong, R.A., Shorter, J.A., Taylor, M.J., Suszcynsky, D.M., et al., 1998. Photometric measurements in the SPRITES '95 and '96 campaigns: nitrogen second positive and first negative emission. J. Atmos. Sol. Terr. Phys. 60, 787.

Astroshop Eu, 2018. Watec Camera. WAT-910HX-RC videokamera.

Barrington-Leigh, C.P., 2001. Identification of sprites and elves with intense video and broadband array photometry. J. Geophys. Res. 106, 1741.

Barrington-Leigh, C.P., Inam, U.S., 1999. Sprites triggered by negative lightning discharges. Journal of Geophysical Research Letters 26, 3605.

Bor, J., 2013. Optically perceptible characteristics of sprites observed in Central Europe in 2007-2009. J. Atmos. Sol. Terr. Phys. 92, 151–177. https://doi.org/10.1016/j.jastp.2012.10.008.

Chen, A, Chen, H, Chuang, C, Cummer, S, Lu, G, Fang, H, et al., 2019. On negative sprites and the polarity paradox. Geophys. Res. Lett. 46, 9370–9378. https://doi.org/10.1029/2019GL083804.

Doug Mink Yale bright Star Catalogue, 2010. Available online at. http://tdc-www.harvard.edu/software/catalogs/bsc5.html.

Franz, C.R., Nemezek, J.R., Winckler, R.J., 1990. Television image of large upward electrical discharge above a thunderstorm system. Science 249 (48).

Frey, H. U, Mende, S. B, Harris, S. E, Heetderks, H, et al., 2016. The imager for sprites and upper atmospheric lightning (ISUAL). J. Geophys. Res.: Space Phys. 121, 8134.

Füllekrug, M., Nnadih, S., Soula, S., Mlynarczyk, J., Stock, M., Lapierre, J., Kosch, M., 2019. Maximum sprite streamer luminosity near the stratopause. Geophys. Res. Lett. 46 https://doi.org/10.1029/2019GL084331.

Hampton, D.L., Heavner, M.J., Wescott, E.M., Sentman, D.D., 1996. Optical spectral characteristics of sprites. Journal of Geophysics Research letters 23 (89).

Heavner, M.J., Morrill, J.S., Siefring, C., Sentman, D.D., et al., 2010. NUV/Blue spectral observations of sprites in the 320-460 region: N2 (2PG) emissions. arXiv: Geophysics.

Hedin, A. E, 1991. Extension of the MSIS thermospheric model into the middle and lower atmosphere. J. Geophys. Res. 96, 1159. https://doi.org/10.1029/90JA02125.

Ihaddadene, M., Celestin, S., 2017. Determination of sprite streamers altitude based on N2 spectroscopicanalysis. J. Geophys. Res.: Space Physics 122, 1000.

Kane, J.A., 1959. Arctic measurements of electron collision frequencies in the D-Region of the Ionosphere. J. Geophys. Res. 64 (113).

Kulak, A., Mlynarczyk, J., 2013. ELF propagation parameters for the ground-ionosphere waveguide with finite ground conductivity. IEEE Trans. Antenn. Propag. 61 (4), 2269–227.

Kulak, A., Kubisz, J., Klucjasz, S., Michalec, A., Mlynarczyk, J., Nieckarz, Z., Ostrowski, M., Zieba, S., 2014. Extremely low-frequency electromagnetic field measurements at the Hylaty station and methodology of signal analysis. Radio Sci. 49, 361–370. https://doi.org/10.1002/2014RS005400.

Kuo, C.L., Hsu, R.R., Chen, A.B., Su, H.T., et al., 2005. Electric fields and electron energies inferred from the ISUAL recorded sprites. Geophys. Res. Lett. 32, L19103.

Liu, N., Dwyer, J.R., Stenbaek-Nielsen, H.C., McHarg, M.G., 2015. Sprites streamer initiation from natural mesospheric structures. Nat. Commun. 29, 7540.

Lyons, W.A., 2015. Electricity in the atmosphere | sprites, Editor(s). In: Gerald, R., John Pyle, North, Zhang, Fuqing (Eds.), Encyclopedia of Atmospheric Sciences, second ed. Academic Press, ISBN 9780123822253, pp. 20–27. https://doi.org/10.1016/B978-0-12-382225-3.00146-8.

Mashao, D. C, Kosch, M. J, Bor, J, Nnadih, S, 2021. The altitude of sprites observed over South Africa. S. Afr. J. Sci. 117 https://doi.org/10.17159/sajs.2021/7941.

Mende, S.B., Rairden, R.L., Swenson, G.R., 1995. Sprite spectra; N2 1 PG band identification. Journal of Geophysics Research 22, 263.

Miyasato, R, Fukunishi, H, Takahashi, Y, Taylor, M. J, 2003. Energy estimation of electrons producing sprite halos using array photometer data. J. Atmos. Sol. Terr. Phys. 65, 573–581. https://doi.org/10.1016/S1364-6826(02)00322-X.

Mlynarczyk, J., Bór, J., Kulak, A., Popek, M., Kubisz, J., 2015. An unusual sequence of sprites followed by a secondary TLE: an analysis of ELF radio measurements and optical observations. J. Geophys. Res. Space Physics 120, 2241–2254. https://doi.org/10.1002/2014JA020780.

Morrill, J., Bucsela, E., Siefring, C., Heavner, M., et al., 2002. Electron energy and electric field estimates in sprites derived from ionized and neutral N2 emissions. Geophys. Res. Lett. 29, 1462.

Neubert, T., Allin, T.H., Stenbaek-Nielsen, H., Blanc, E., 2001. Sprites over Europe. Geophys. Res. Lett. 28, 3585.

Neubert, T., Rycroft, M., Farges, T., Blanc, E., et al., 2008. Recent results from studies of electric discharges in the mesosphere. Surv. Geophys. 29, 71.

Nnadih, S., Kosch, M., Martinez, P., Bor, J., 2018. First ground-based observations of sprites over southern Africa. South African Journal of Science, 9/10 84.

Sato, M.T., Ushio, T., Morimoto, M., Kikuchi, et al., 2015. Overview and early results of the global lightning and sprite measurements mission. J. Geophys. Res.: Atmosphere 120, 3822.

Sentman, D.D., Wescott, E.M., Osborne, D.L., Hampton, D.L., et al., 1995. Preliminary results from the sprites94 campaign: red sprites. Journal of Geophysical Research Letters 22, 1205.

Soula, S, Van der Velde, O, Montanya, J, Neubert, T, Chanrion, O, Ganot, M, 2009. Analysis of thunderstorm and lightning activity associated with sprites observed during the EuroSprite campaigns: Two case studies. Atmos. Res. 91, 514–528. https://doi.org/10.1016/j.atmosres.2008.06.017.

Surkov, V.V., Hayakawa, M., 2012. Underlying mechanisms of transient luminous events: a review. Ann. Geophys. 30, 1185.

Suszcynsky, D.M., Roussel-Dupre, R., Lyons, W.A., Armstrong, R.A., 1998. Blue light imagery and photometry of sprites. J. Atmos. Sol. Terr. Phys. 60, 801.

Suzuki, T., Hayakawa, M., Matsudo, Y., Michimoto, K., 2006. How do winter thundercloud systems generate sprite-induced lightning in the Hokuriku area of Japan? Geophys. Res. Lett. 33 (10), 467.

Takahashi, Y, Yoshida, A, Sato, M, Adachi, S, Kondo, R, Hsu, R, et al., 2009. Absolute optical energy of sprites and its relationship to charge moment of parent lightning discharge based on measurement by ISUAL/AP. J. Geophys. Res., 115, A00E55. https://doi.org/10.1029/2009JA014814.

Tec, 2019. Maxwell-Boltzmann distribution. Available at. https://www.tec-science.com/thermodynamics/kinetic-theory-of-gases/maxwell-boltzmann-distribution/. Accessed 05/08/2020.

Williams, E. R, Lyons, W. A, Hobara, Y, Mushtak, V. C, et al., 2010. Ground-based detection of sprites and their parent lightning ashes over Africa during the 2006 AMMA campaign. J. R. Meteorol. Soc. 136, 257.

Winckler, J.R., Lyons, W.A., Nelson, T.E., Nemzek, R.J., 1999. New high-resolution ground-based studies of cloud-ionosphere discharges over thunderstorms. Journal of Geophysics Research letters 101, 6997.

Yair, Y., PIsraelevich, D. A. Devir, Moalem, M., et al., 2004. New observations of sprites from the space shuttle. Journal of Geophysics Research letters 109, 34.

Yaniv, R., Yair, Y., Price, C., Bor, J., et al., 2013. Ground-based observations of the relations between lightning charge-moment-change and the physical and optical properties of column sprites. J. Atmos. Sol. Terr. Phys. 107, 60.